



# Evaluation of Sensitization Behaviors on the Heat-Affected Zone of Austenitic Stainless Steel Weld by Thermal Cycles of Actual Multi-pass Welding

Gidong Kim<sup>1</sup> · Junho Lee<sup>2</sup> · Seunghyun Kim<sup>1</sup> · Yongjoon Kang<sup>1</sup> · Jun-Yong Park<sup>2</sup> · Sang-Woo Song<sup>1</sup> 

Received: 12 December 2023 / Accepted: 13 March 2024  
© The Author(s) 2024

## Abstract

The sensitization behavior of the welding heat affected zone (HAZ) in austenitic stainless steels (SSs) was investigated through simulated thermal cycles emulating actual multi-pass welding processes using the Gleeble simulator. The tests were performed with austenitic SSs, considering carbon contents, heat input, and distance from the fusion line to determine the thermal cycle conditions of the HAZ. Higher carbon content led to increased sensitization (degree of sensitization, DOS) values, while the influence of the thermal cycle in the final weld pass was that even though it was rapidly heated to over 1000 °C and cooled at a rapid rate, the DOS value decreased due to partial carbide dissolution and chromium diffusion. Therefore, effective management of the final thermal cycle in the HAZ contributes to improved intergranular stress corrosion cracking resistance. Even with prolonged exposure of the HAZ to the sensitization region, the discovery that corrosion resistance improves when the final heating cycle reaches 1000 °C underscores the importance of HAZ heat cycle management and provides valuable insights for materials engineering and industrial applications.

**Keywords** Sensitization · Austenitic stainless steel · Heat affected zone · Gleeble · DL-EPR test

## 1 Introduction

Austenitic stainless steels (SSs), known for their excellent corrosion resistance and mechanical properties, have been widely used in many industrial plant components, including

nuclear power plants. However, when exposed to a high-temperature range of 400–800 °C during heat treatment and welding processes, chromium (Cr) near the grain boundary may be depleted due to carbide precipitation, leading to a state of sensitization [1]. If sensitized, grain boundaries corrosion resistance would be reduced and materials become more vulnerable to intergranular stress corrosion cracking (IGSCC) [2, 3]. In this regard, a wide range of studies have been conducted on the sensitization behaviors of austenitic SSs using various test methods. Among these methods, oxalic acid etching test (ASTM A 262) could provide qualitative evaluation. Meanwhile, the double loop-electrochemical potentiokinetic reactivation (DL-EPR) test (ASTM G 108) could be used for the quantitative assessment of sensitization [2–7]. The sensitization mechanism is established through extensive research [8–10].

The sensitization is not a concern for austenitic SS welds which contain a certain amount of delta ferrite phase [11]. However, it would be challenging to predict sensitized regions when the thermal cycles of the welding heat-affected zone (HAZ) are complex and diverse, as in the case of multi-layer welding. AISI 304 austenitic SS showed no signs of sensitization in a single-pass welding HAZ. In contrast, a

---

✉ Sang-Woo Song  
swsong@kims.re.kr

Gidong Kim  
gdkim@kims.re.kr

Junho Lee  
jhlee88@kims.re.kr

Seunghyun Kim  
skims@kims.re.kr

Yongjoon Kang  
yjkang@kims.re.kr

Jun-Yong Park  
leopark17@kims.re.kr

<sup>1</sup> Joining Technology Department, Korea Institute of Materials Science, Changwon 51508, Republic of Korea

<sup>2</sup> Authorized Nuclear Inspection Department, Korea Institute of Materials Science, Changwon 51508, Republic of Korea

sensitization region of approximately 3 mm was found notably across the grain coarsening zone in double-pass welding [12]. This sensitization is extended to a maximum of 5 mm in the case of triple-pass welding. For type 1.4003 steel, a low carbon SS variant with 12% chromium ferritic SS, sensitization was only observed when the HAZ between the welding passes overlapped, and the locations subjected to sensitization varied depending on differences in the heat input [13]. In addition, it was observed that a subsequent decrease in mechanical properties due to the grain refinement caused by recrystallization in the HAZ and changes in the delta ferrite morphology occurred as the accumulated heat input increased [14, 15]. Despite these types of research, sensitization behavior within the multi-layer welding HAZ of austenitic SSs according to the actual multi-pass welding process which have over 20 passes was inadequately understood.

In this regard, the sensitization behavior of the welding HAZ of austenitic SSs, depending on the carbon content and heat input, was investigated by simulating the welding HAZ's thermal cycles through the actual multi-pass welding process. Due to the exceedingly narrow range of the welding HAZ, typically spanning a few millimeters, the Gleeble simulator has been successfully utilized to accurately control the thermal cycles and heat input to easily simulate an available HAZ for the evaluation of the microstructure and mechanical properties [16, 17]. In this paper, we attempted to present a methodology to discover the most vulnerable area by quantifying the degree of sensitization of the HAZ area during multi pass welding, which is frequently performed in actual multi-pass welding in the process of manufacturing pressure vessels or pressure piping. HAZ simulation test pieces were produced using the Gleeble simulator based on the actual measured thermal cycle of actual multi-pass welding. DL-EPR test was used to evaluate the sensitization behavior. The sensitization behavior of HAZ related to thermal cycles was observed, and the results were discussed, given the effect of carbon content and heat input on the sensitization behavior of 304 austenitic SS in each HAZ area.

## 2 Materials and Experiments

### 2.1 Test Materials

In this study, three types of 304 stainless steels with different carbon contents were utilized to quantitatively evaluate the

sensitivity of the heat-affected zone (HAZ) to variations in carbon content. The chemical compositions of the test materials which analyzed using ICP-AES (inductively coupled plasma atomic emission spectroscopy) are summarized in Table 1. For measuring the thermal cycle at different HAZ locations, K-type thermocouples were attached at intervals of 1.5–2 mm on the inner and outer surfaces of A240 304H austenitic stainless steel plates with a thickness of 15 mm, as shown in Fig. 1. These plates were used only to check the thermal cycle of the HAZ and were not related to the specimens for Gleeble tests on which the chemical composition analysis was performed. Welding was performed using a 2.4 mm diameter ER308L filler rod for gas tungsten arc welding (GTAW) multi-pass welds. The welding procedure specification (WPS) based on the KEPIC standard welding procedure (KEPIC SWPS-0808-GT-02, Rev.0) was employed for welding, and detailed welding conditions are presented in Table 2, with 11 layers and 21 passes deposited in the welding process. To compare the microstructure of the weld HAZ with simulated specimens, the microstructure of the HAZ of the actual welded coupon was collected 4 mm away from the fusion line.

The thermal cycle of the HAZ was simulated using a Gleeble 3800 (Dynamic System Inc.) welding simulator with a maximum heating rate of 104 °C/s. The mounting configuration of the Gleeble specimen for the simulation of HAZ thermal cycles is shown in Fig. 2. Feedback signals required for closed-loop control are collected from thermocouples welded at the center of the specimen. Three types of austenitic stainless steels with varying carbon contents were machined into 6 mm diameter rod-shaped models to simulate the thermal cycle based on HAZ location and input heat.

### 2.2 Test Methods for Evaluation of Sensitization Behavior on HAZ

Quantitative and qualitative analyses were employed to evaluate the sensitization behavior of specimens with simulated heat histories using the Gleeble testing machine. The test conditions are summarized in Table 3. The samples with simulated heat histories were prepared where the central region of the model, accurately reproducing the heat history, was polished to 1 µm for quantitative assessment of the degree of sensitization (DOS) according to ASTM G108 [3]. The specimens were prepared using #600, #1200, #2400 grit emery sheets, followed by a final

**Table 1** Chemical composition of test materials (wt%)

Materials	C	Si	Mn	Cr	Ni	P	S	N
A240 304L	0.018	0.40	1.63	18.10	8.20	0.033	0.002	0.07
A240 304H	0.048	0.34	1.45	18.16	8.09	0.035	0.001	0.07
A182 F304H	0.074	0.45	1.41	18.53	8.44	0.031	0.013	–

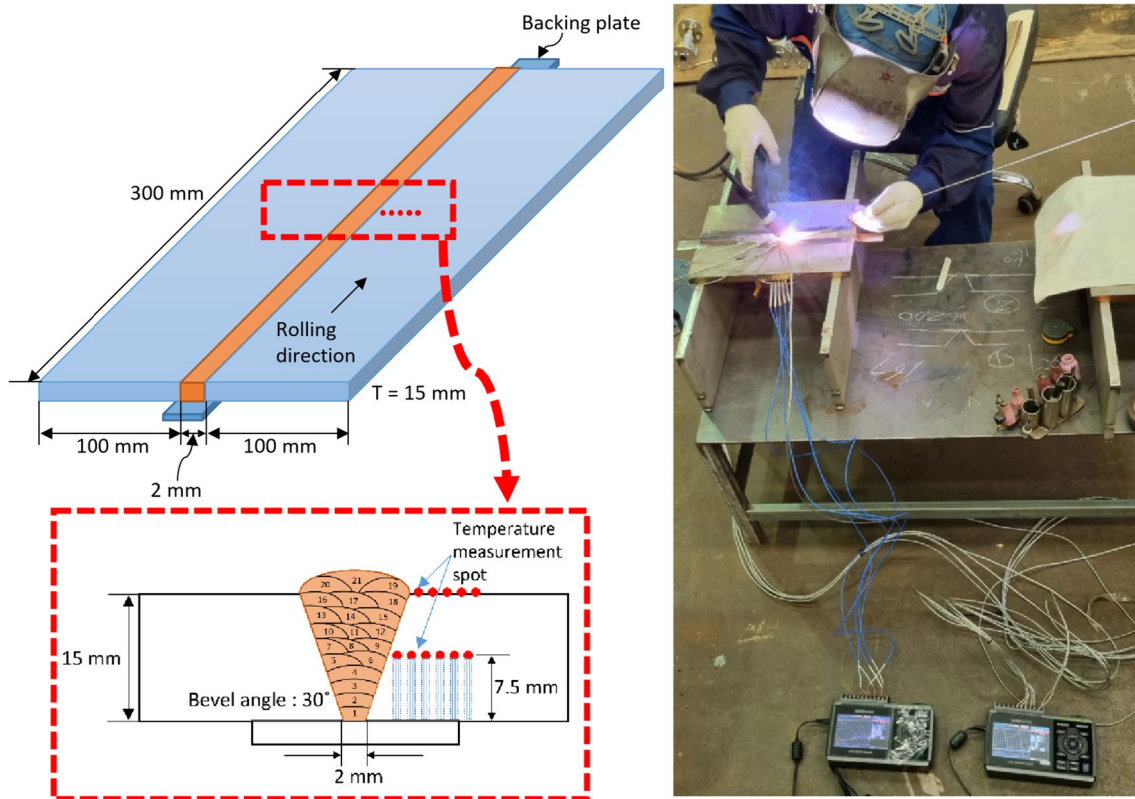


**Fig. 1** Thermal cycle measurement by welding heat-affected zone location

**Table 2** Welding conditions applied to the production of welding coupons

Preheat (low heat input/high heat input)				
Minimum preheat temperature (°C)	10			
Interpass temperature (°C)	167/300–400			
Gas				
Shielding gas	Type	Purity (%)	Flow rate (l/min)	
	Ar	99.99	7–20	
Heat input	Current (A)	Voltage (V)	Travel speed (cm/min)	Heat input (kJ/cm)
Electrical characteristics (Low heat input/high heat input)				
Root	120/236	11/16	7/15	11.3/15.1
Fill	185/290	14/20	9/14	17.3/24.4
Current or polarity	DCEN			

polishing with 1  $\mu\text{m}$  diamond suspension (ALLIED). A double-loop electrochemical potentiodynamic reactivation (DL-EPR) test was performed for DOS quantification. The electrochemical tests were conducted using a potentiostat/impedance analyzer (Gamry Reference 600+), a 500 mL volume corrosion cell, an Ag/AgCl (saturated KCl) reference electrode, and a Pt counter electrode. Test solutions were 0.5 M  $\text{H}_2\text{SO}_4$  + 0.01 M KSCN, and open circuit potential (OCP) was measured to obtain a steady

state in all tests with potentiodynamic electropolarization sequentially measured. The DOS was calculated as the ratio of  $I_r/I_a$ , where  $I_r$  represents the peak reactivation current density and  $I_a$  represents the peak activation current density. To determine  $I_a$ , the specimen was anodically polarized at 0  $V_{\text{OCP}}$  below the open-circuit potential (OCP) at a scan rate of 0.833 mV/s (vertex potential =  $0.5V_{\text{ref}}$ , final potential =  $-0.3V_{\text{OCP}}$ ), and the applied potential was then reversed to determine  $I_r$ .

**Fig. 2** Insertion of the specimen inside the Gleeble simulator

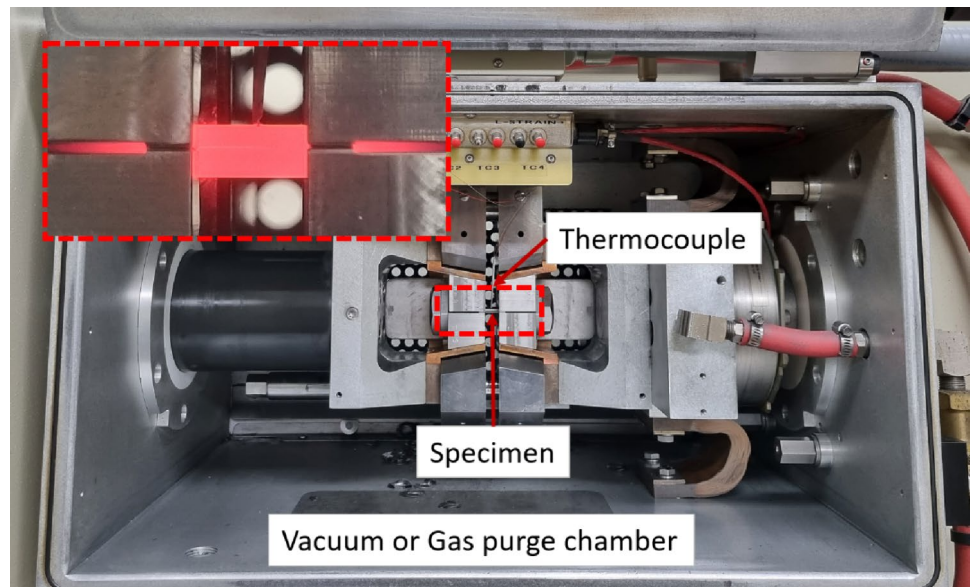


**Table 3** Test condition for evaluating sensitization behavior

Test materials	A240 304L, A240 304H, A182 F304H
Heat input	(Low) 17.3 kJ/cm, (High) 24.4 kJ/cm
Distance from the fusion line related to thermal cycles	1 mm, 4 mm, 7 mm
Sensitization test	
DL-EPR test (ASTM G108)	A scan rate of 0.833 mV/s in 0.5 M H <sub>2</sub> SO <sub>4</sub> + 0.01 M KSCN solution at RT
Oxalic acid etching test (ASTM 262 practice A)	10% H <sub>2</sub> C <sub>2</sub> O <sub>4</sub> + 2H <sub>2</sub> O for 1.5 min at 1 A/cm <sup>2</sup>

For qualitative sensitization evaluation in the test material, oxalic acid etching tests were conducted according to ASTM A262 practice A [2]. The polished samples were exposed to 10 wt% oxalic acid crystals (H<sub>2</sub>C<sub>2</sub>O<sub>4</sub>·2H<sub>2</sub>O) in distilled water solution at a current density of 1 A/cm<sup>2</sup> for 1.5 min. The etched microstructures were observed using an optical microscope (OM) and classified following the guidelines outlined in ASTM A262 practice A. Additionally, after the DL-EPR test, the microstructure was observed using scanning electron microscopy (SEM, 20 kV, JEOL JSM-7001F), and a transmission electron microscope (TEM, 200 kV, JEOL JEM 2100) equipped with Energy Dispersive Spectroscopy (EDS) was used to compare and analyze the chromium carbides in the heat-affected zone of actual welded coupons and the simulated heat history specimens.

### 3 Results and Discussion

#### 3.1 Thermal Cycles of HAZ in the Actual Multi-pass Welding

The thermal cycle required to produce a HAZ simulation specimen can be obtained through finite-element analysis software or direct measurement using a thermocouple during welding. In this study, we used direct heat history measurements since actual welding data are necessary for highly reliable welding condition settings. The results are shown in Fig. 3. Welding was performed under two heat input conditions: low heat input at 17.3 kJ/cm and high heat input at 24.4 kJ/cm. Temperatures were measured at varying distances to the fusion line from the center (approximately 7.5 mm from the surface in the thickness direction) and the surface of the specimen. It would be observed that the maximum exposed temperature of the heat-affected zone is higher and closer to the fusion line and that there is significant variation in the maximum temperature at different locations.

While there are differences in the maximum exposed temperatures at each location, it was confirmed that



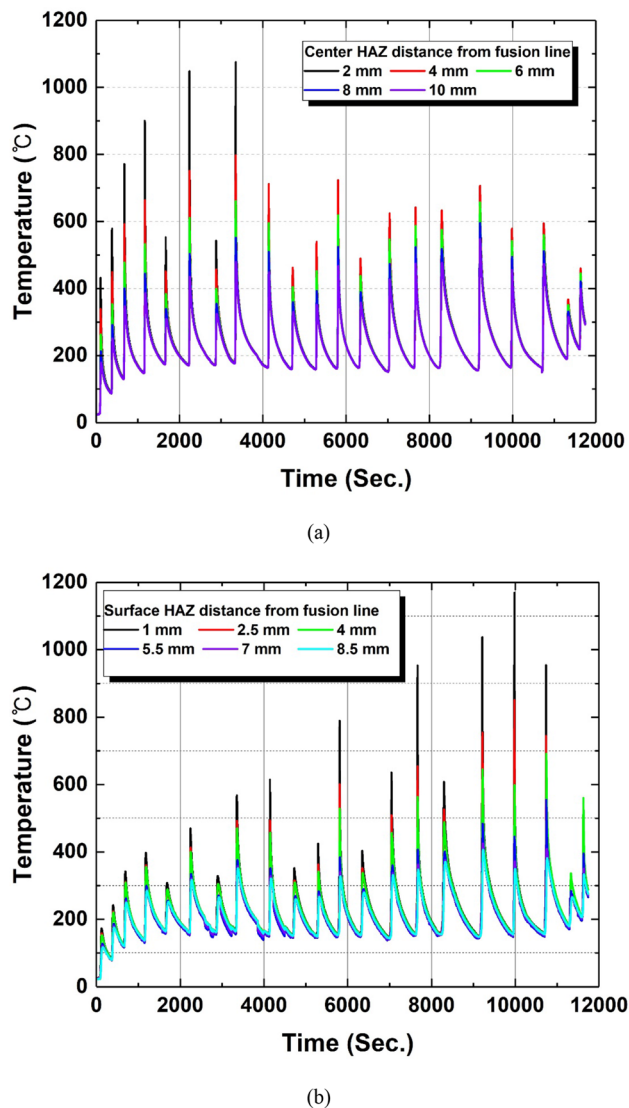


**Fig. 3** Thermal cycle measurement results at the **a** center and **b** surface HAZ area of base metal

thermal cycles remain consistent even if the distance is far from the fusion line. As in previous studies, the variation in microstructural characteristics within the HAZ area is due to the different maximum temperatures and exposure times at other HAZ locations [18]. Additionally, while the center of the specimen in the thickness direction exhibits a distribution of temperatures exceeding 600 °C within a relatively short time, the surface shows an extended period (over 5000 s) of high-temperature diffusion. This indicates differing temperature and time domains exposed in the thickness direction, likely influenced by the distance from the heat source [19]. Therefore, given the variation in exposed thermal cycles based on thickness direction and HAZ location, it can be inferred that the sensitization behavior related to carbon content will also differ.

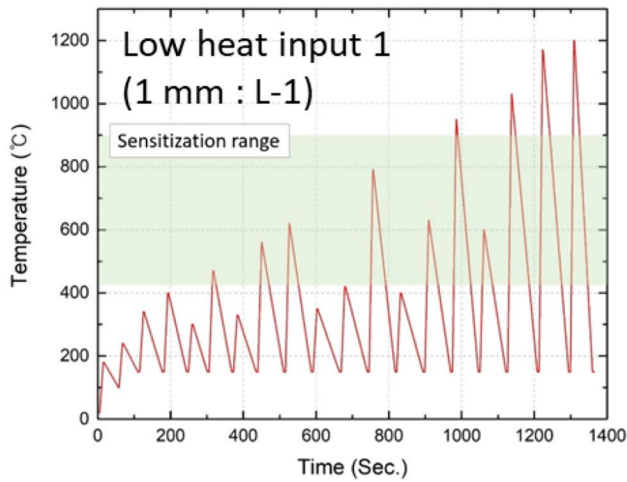
In this study, specimens were prepared to evaluate the susceptibility to corrosion and IGSCC caused by sensitization behavior by selecting heat history conditions on the material surface, as corrosion and IGSCC mainly occur on the surface. The susceptibility of the HAZ region at different positions on the surface was then assessed.

### 3.2 Gleeble Simulation of the Thermal Cycles of Actual Weld HAZ

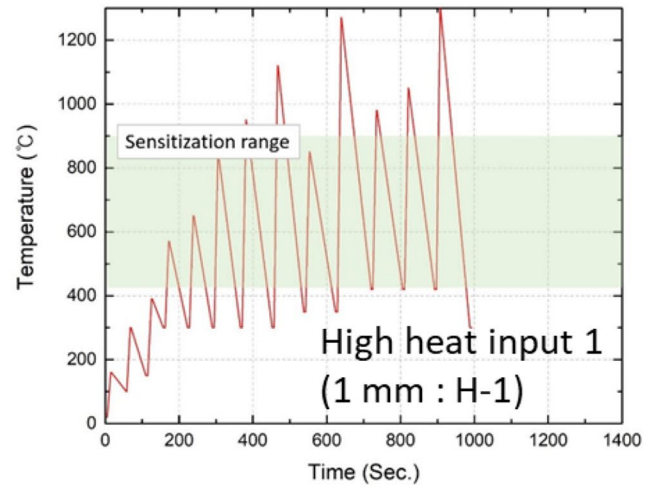
Based on the measured heat histories at different positions on the surface HAZ, the conditions for the Gleeble test machine were established, as shown in Fig. 4. For both low heat input and high heat input conditions, heat histories were selected at distances of 1 mm, 4 mm, and 7 mm from the end of the fusion line. As the exposure time increases due to the surface HAZ heat history conditions, higher temperature ranges are reached, and as the distance from the weld joint increases, the maximum temperature decreases. Furthermore, the high heat input condition at different positions on the weld joint reaches temperatures exceeding 600 °C faster than the low heat input condition, indicating a relatively shorter overall heat history exposure time. Previous studies confirmed the sensitization temperature range and the precipitation rate of Cr-rich  $M_{23}C_6$  carbides at grain boundaries for 18Cr-9Ni stainless steel based on carbon content [20]. Sensitization generally occurs in the range of 420–800 °C, which was incorporated into the thermal cycle of the Gleeble test machine. Among the conditions, the high heat input condition (H-1) located 1 mm from the fusion line experienced the longest exposure time in the temperature range where sensitization occurs. On the other hand, the low heat input condition (L-3) positioned 7 mm away from the fusion line was not exposed to the sensitization temperature range. While the low heat input condition (L-2) placed 4 mm away from the fusion line and the high heat input condition (H-3) located 7 mm away from the fusion line were exposed to the sensitization temperature range, the short exposure times suggest that sensitization is unlikely to occur. On the contrary, specimens of L-1, H-1, and H-2 conditions exposed to the sensitization temperature range for relatively extended periods are expected to exhibit sensitization behavior.

### 3.3 Microstructure of the Actual Welding and Simulated Specimens

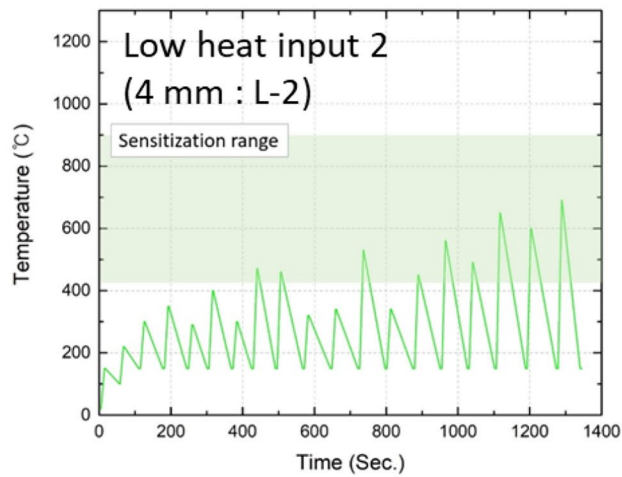
To confirm the replicability of the HAZ in the Gleeble specimen, a comparative analysis was conducted between the microstructure of the production weld HAZ and that of the simulated model subjected to an H-2 condition. In conventional multi-pass welding, sensitization was reported to occur within the HAZ region at a distance of 3–5 mm [12]. Thus, a comparison was made at the 4 mm location,



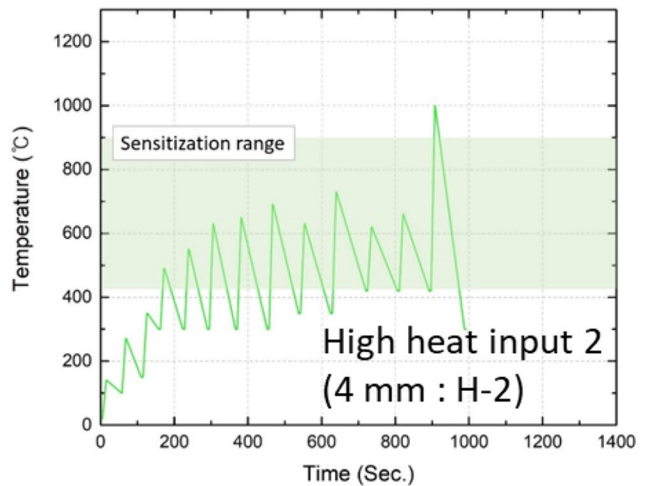
(a) L-1: Low heat input, 1 mm away from the fusion line.



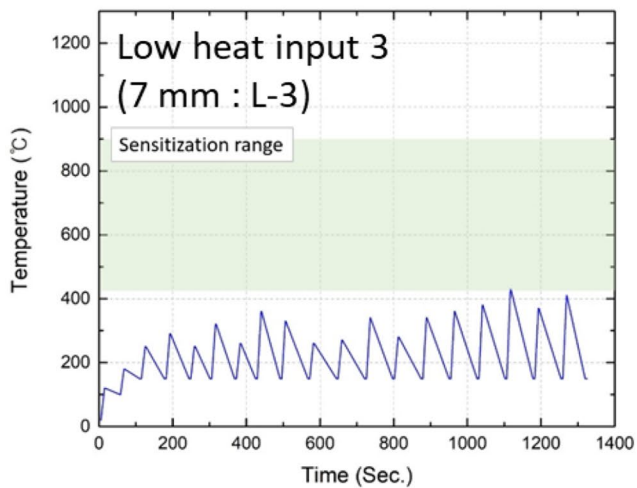
(d) H-1: High heat input, 1 mm away from the fusion line.



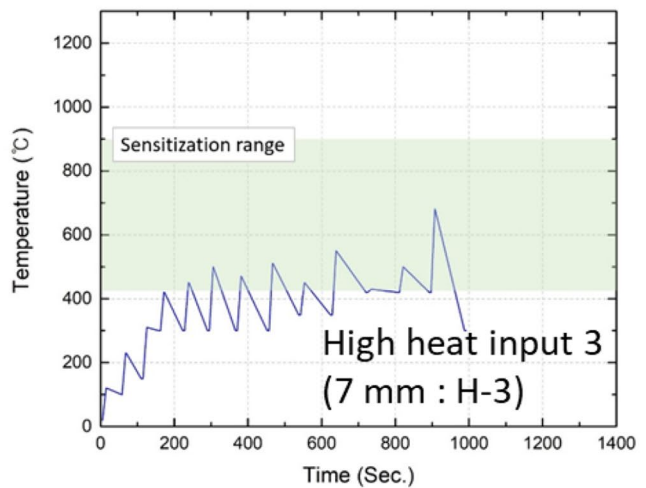
(b) L-2: Low heat input, 4 mm away from the fusion line.



(e) H-2: High heat input, 4 mm away from the fusion line.



(c) L-3: Low heat input, 7 mm away from the fusion line.



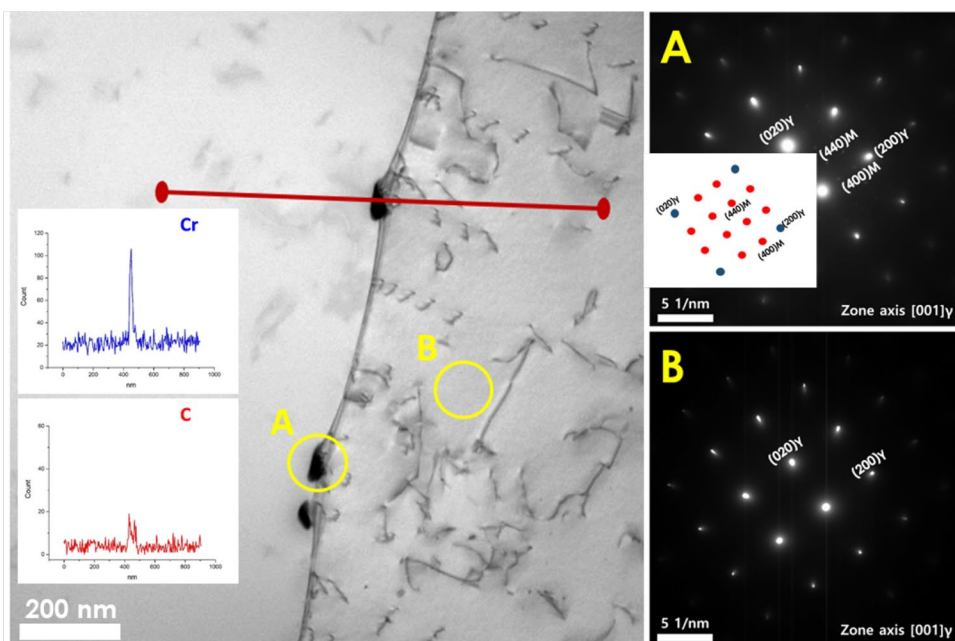
(f) H-3: High heat input, 7 mm away from the fusion line.

**Fig. 4** Gleeble thermal cycle conditions for HAZ simulation by heat input and distance from fusion line: **a** L-1, **b** L-2, **c** L-3, **d** H-1, **e** H-2, **f** H-3

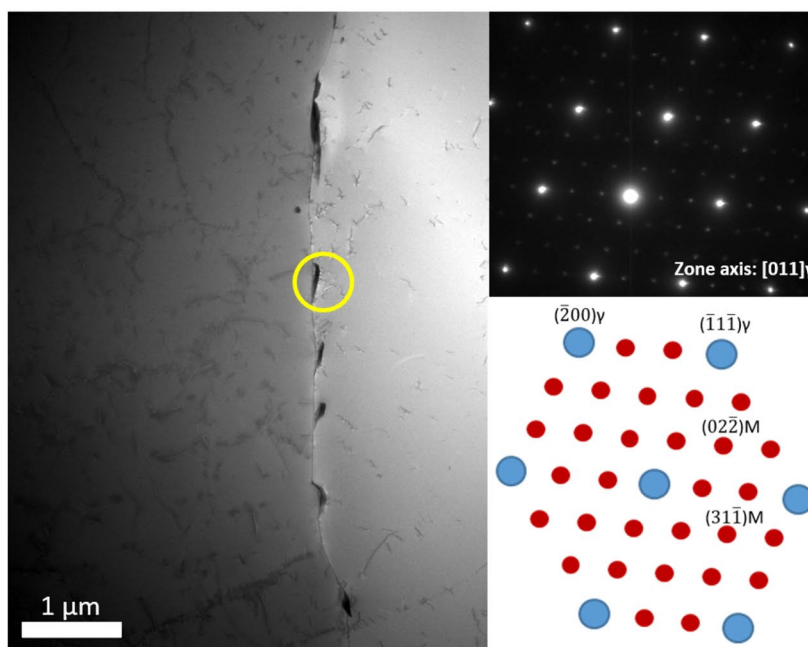
designated as condition H-2, to confirm the sensitization indicated by chromium carbides at the grain boundary. Figure 5 illustrates the TEM microstructures of the actual welded HAZ and the Gleeble-simulated specimens. Figure 5a is the high heat input condition of 304H material in the area 4 mm away from the fusion line. Figure 5b is the high heat input condition of F304H material simulated using Gleeble simulator with having thermal cycle of 4 mm away from the fusion line. The selected area diffraction (SAD)

patterns of Points A and B in Fig. 5a were observed along the zone axis of  $[001]_{\gamma}$ . The clear presence of  $(020)_{\gamma}$  and  $(200)_{\gamma}$  miller indices in both Points A and B indicates the presence of an austenite matrix. At Point A, located within the grain boundary region containing precipitates,  $(440)_{\text{M}}$  miller indices were identified in addition to austenite. This corresponds to the  $\{110\}$  orientation and signifies the presence of  $\text{M}_{23}\text{C}_6$  precipitates containing carbon [21]. Further EDS line scans confirmed the high carbon and chromium

**Fig. 5** TEM micrographs, SAD pattern, and EDS line scan of **a** production weld HAZ and **b** simulated specimen of H-2 condition



(a)



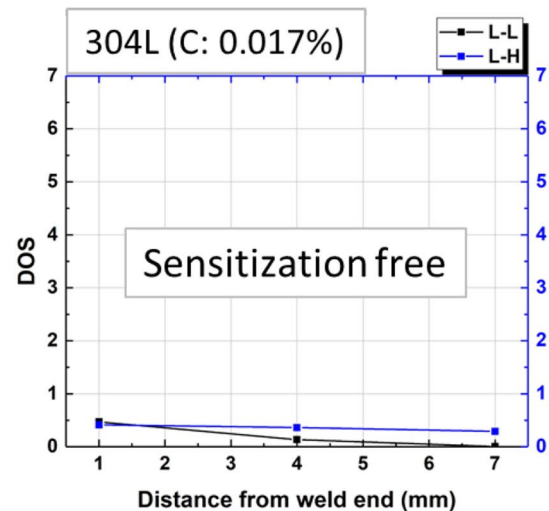
(b)

**Fig. 6** DL-EPR test results according to distance from weld end (mm) and carbon content **a** 304L, **b** 304H, and **c** F304H

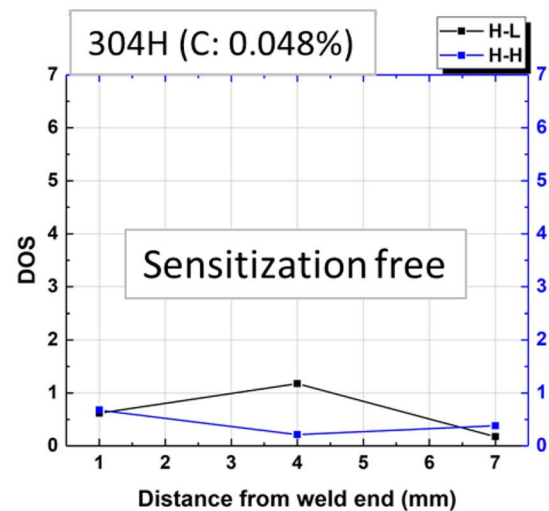
content, signifying the nature of these residues as chromium carbides. This finding indicates the presence of  $M_{23}C_6$  carbides precipitated along the austenite boundaries. Furthermore, in the SAD pattern of the Gleeble specimen simulated under the same heat history, as shown in Fig. 5b, the presence of  $M_{23}C_6$  precipitates across the austenite grain boundaries could be observed through the  $\{110\}$  orientation. This demonstrates that the thermal cycle simulation performed using the Gleeble simulator had been accurately executed. It could be observed that  $M_{23}C_6$  carbides have precipitated along the boundaries of the austenite phase. Similarly, in the SAD pattern of the Gleeble-simulated specimen with the same thermal cycles,  $M_{23}C_6$  carbides are seen to precipitate at the austenite grain boundaries, demonstrating that the thermal cycle simulation by the Gleeble simulator has been accurately executed. The carbon content of the austenitic SS used as a comparative material was 0.074 wt%. According to the Time–Temperature–Sensitization (TTS) diagram, chromium carbides precipitate at around 680 °C for approximately 100 s and around 550 °C for about 1000 s [20]. The thermal cycles recorded by the Gleeble simulator closely replicated the thermal cycles of the actual weld HAZ, and the exposure time at temperatures above 550 °C was relatively short, around 220 s, and varied. It is deduced that had the Gleeble simulator not accurately simulated the thermal cycles, chromium carbide would not have been precipitated. The high heat input condition (H-2) thermal cycle positioned 4 mm away from the fusion line exhibits active precipitation of  $M_{23}C_6$  carbides along the grain boundaries, as mentioned in the preceding section. This indicates a correlation between the exposure time to the sensitization range and the enhanced precipitation of  $M_{23}C_6$  carbides at the grain boundaries, suggesting a significant influence on sensitization behavior at the austenite grain boundaries.

### 3.4 Sensitization Behavior of HAZ

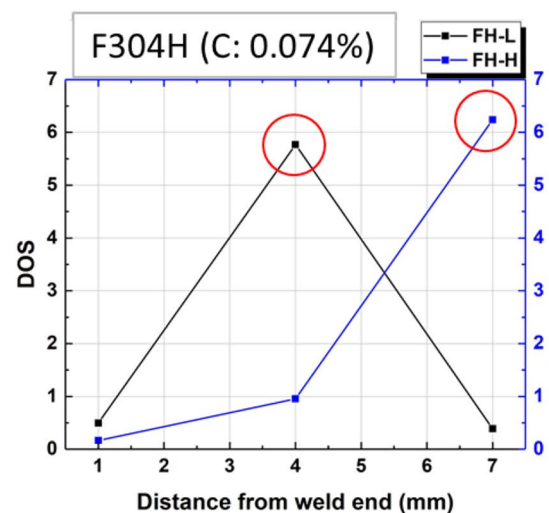
Figure 6 presents the results of the DL-EPR tests conducted on the simulated Gleeble specimen for the weld HAZ of different positions concerning carbon content and heat input. The low and high heat input conditions for 304L were designated as L–L and L–H, respectively. Similarly, for 304H, the conditions were indicated as H–L and H–H, while for F304H, they were denoted as FH–L and FH–H. For 304L with lower carbon content, under the low heat input condition, the DOS values for all positions in the HAZ were less than 0.5, indicating the absence of sensitization. Under the high heat input condition, all areas of the HAZ had DOS values slightly higher than those of the low heat input condition, yet the values remained very small and below 1. This



(a)



(b)



(c)

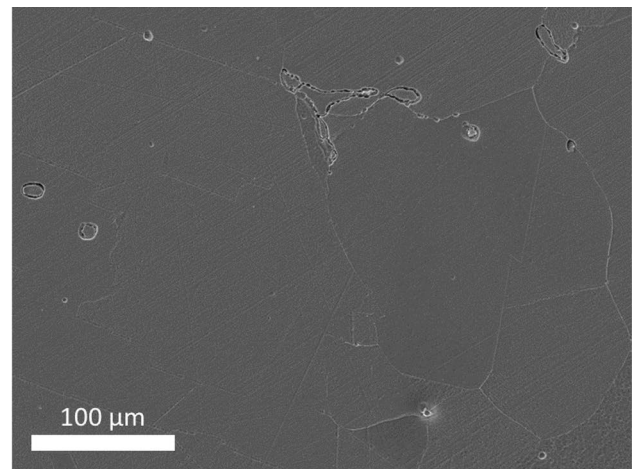


indicates that regardless of the heat input, sensitization does not occur when the carbon content is low. In the case of 304H, which has a slightly higher carbon content than 304L, the DOS values exhibited a minor increase under common heat input conditions; nevertheless, they remained generally below 1, confirming the absence of sensitization.

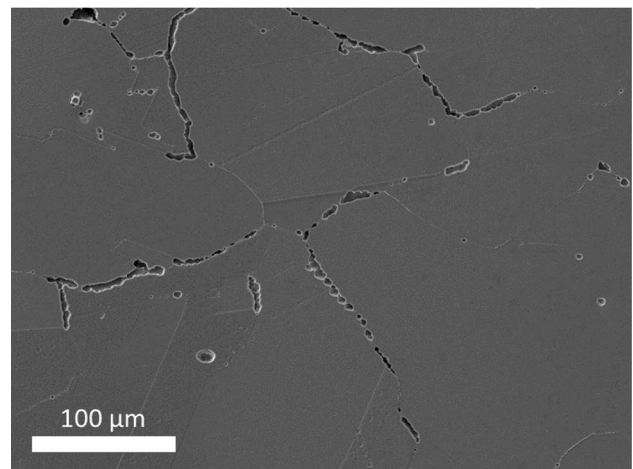
However, in contrast to the previous DL-EPR findings for 304L, the situation differed for 304H. The DOS value showed an elevation under the thermal cycle condition at a distance of 4 mm from the weld, even with low heat input conditions. This phenomenon could be attributed to the final cycle peak of the thermal cycle, which reached approximately 1000 °C and is recognized as the austenitization temperature [22, 23]. Moreover, L-1 and H-1 conditions, representing thermal cycle states at distances of 1 mm from the weld, had a lengthier exposure, within the sensitization temperature range, than L-2 and H-2 conditions. However, during the later phases of the thermal cycle, these regions encountered relatively higher solution annealing (SA) temperatures, resulting in the depletion of precipitated carbides. As a result, it is anticipated that the DOS values would not exhibit significant elevation [24]. This pattern corresponds with the observed behavior in low carbon content 304L. Nevertheless, the general SA temperature surpasses 1050 °C, exceeding the final cycle peak temperature of the H-2 condition, and the duration of exposure is also briefer. Consequently, the explanation could not be solely attributed to temperature ranges. This aspect will be explored further in the subsequent section.

Similar behavior of DOS values to that of 304H was also observed in F304H with higher carbon content. Under the thermal cycle conditions 1 mm away from the weld joint in the HAZ (H-1, L-1), despite prolonged exposure in the sensitization temperature range, sensitization did not occur with DOS values remaining below 1, regardless of the heat input. This trend aligns with the behavior of 304L and 304H. Furthermore, under the high heat input thermal cycle condition (H-2) located 4 mm away from the weld joint, the DOS value was lower than that of the low heat input thermal cycle condition (L-2), while under the high heat input thermal cycle condition (H-3) positioned 7 mm away from the weld joint, the DOS value was higher than that of the low heat input thermal cycle condition (L-3). As shown in Fig. 7a, the microstructure under condition L-1 after DL-EPR testing of F304H showed no evidence of grain boundary sensitization. Still, under condition L-2, sensitization at the grain boundaries was observed. Additionally, etching tests were conducted for qualitative observation, and the results are presented in Fig. 7b. Consistent with the described tendency, condition L-2 was categorized as a 'dual structure' due to high DOS values.

In contrast, condition L-1, despite more prolonged exposure in the sensitization temperature range, was classified as



(a)



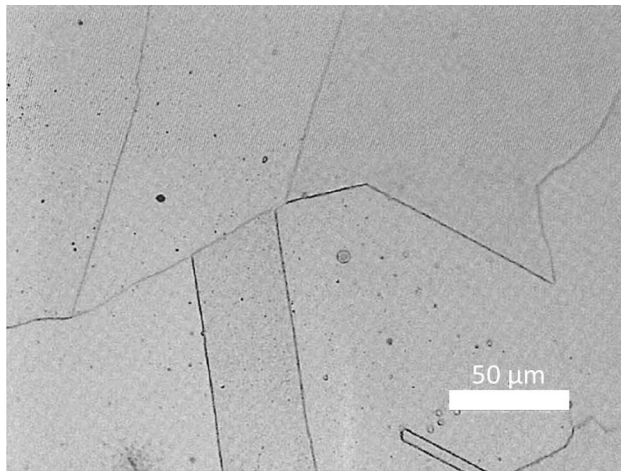
(b)

**Fig. 7** SEM micrographs after DL-EPR tests of simulated specimens of **a** FH-L-1 (DOS 0.49) and **b** FH-L-2 (DOS 5.77) conditions

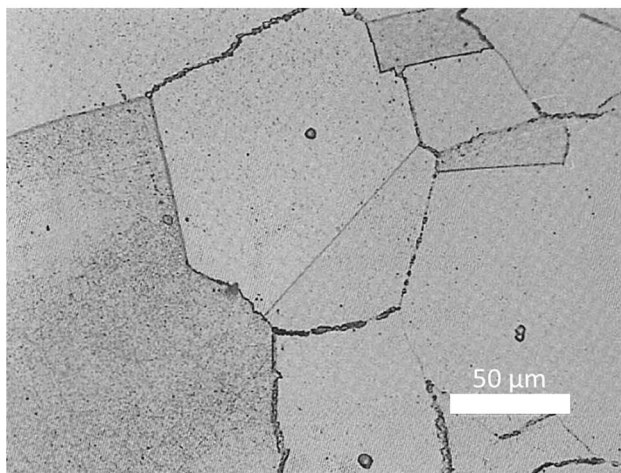
'end grain I' due to lower DOS values, as shown in Fig. 8. For the L-3 thermal cycle condition, exposure did not reach the sensitization temperature range. However, for the H-3 thermal cycle condition, the DOS value was higher than the exposure time in the sensitization temperature range. Due to higher carbon content than 304H, significant carbides precipitated at grain boundaries even with shorter exposure times, leading to higher DOS values. The tendency for the time required for chromium carbide precipitation based on temperature to decrease with higher carbon content is consistent with the TTS diagram [20].

### 3.5 Identification of the Last Cycle Peak Effect of Thermal Cycles by DL-EPR Test

As shown in Fig. 9, the last cycle peak effect was investigated by applying the previous cycle peak condition of



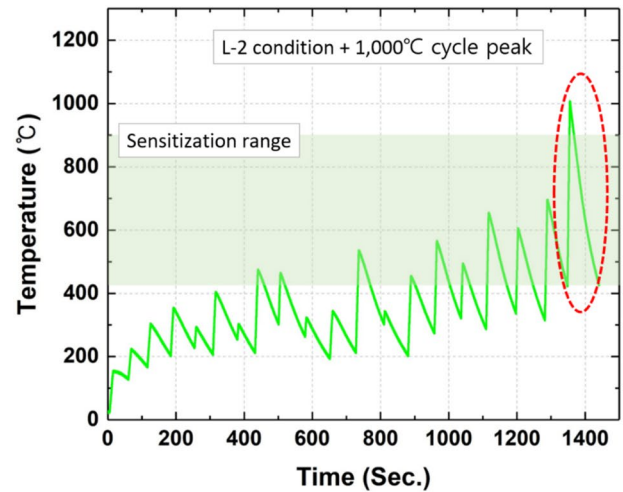
(a)



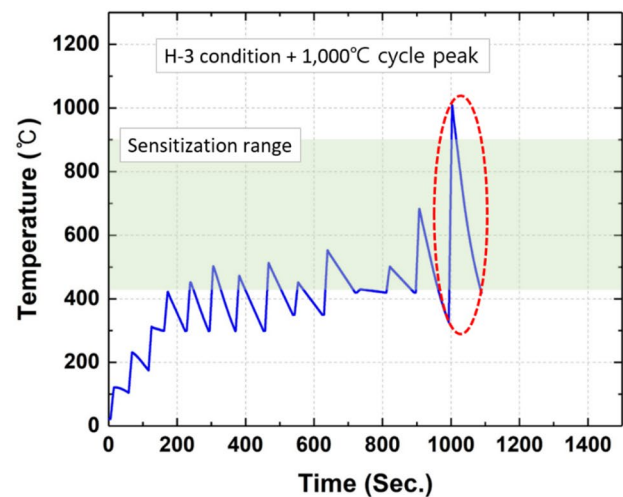
(b)

**Fig. 8** Oxalic etching test results of **a** FH-L-1 and **b** FH-L-2 conditions

H-2 to the thermal cycle of L-2 and H-3 for F304H, where sensitization had occurred. Using the Gleeble simulator, test specimens were fabricated by applying the thermal cycle conditions of L-2 and H-3 with an additional last cycle peak at 1000 °C to F304H specimens. The DL-EPR test was conducted in the same manner as previously described, and the results are shown in Fig. 10a, b. It could be observed that the DOS values reduced to 2 or below in the conditions with the applied 1000 °C last peak. As a general understanding, increasing the austenitization temperature to 1100 °C promotes the dissolution of carbides and chromium enrichment in the matrix [22, 23]. Although characterized by a relatively lower temperature and a brief duration, the last cycle peak still exhibits this phenomenon. Previous studies experimentally demonstrated that even with rapid heating and cooling at a rate of 200 °C/s to 950 °C (holding for 2 s) followed by limited diffusion time, short-range diffusion occurs, and



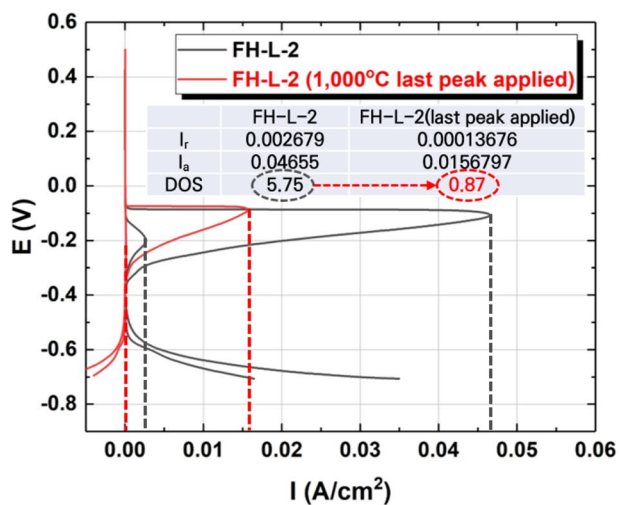
(a)



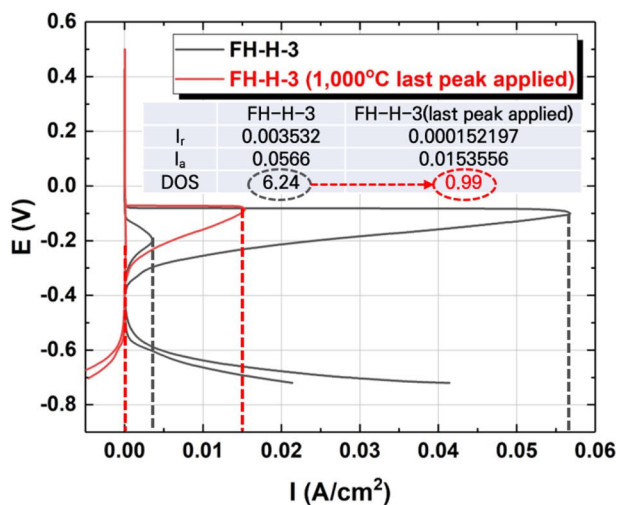
(b)

**Fig. 9** Gleeble thermal cycle conditions with 1000 °C last cycle peak for **a** L-2 and **b** H-3

partial carbide dissolution has been observed in fine carbides [25]. Given that the last cycle peak is attained at a slower heating rate of approximately 90 °C/s compared to prior research and at a higher temperature, it is anticipated that the extent of dissolution and the diffusion of chromium would be more active. Additionally, with a cooling rate of 8 °C/sec, the process can be safely followed without risking further sensitization [24]. Although the peak temperature and exposure time for a complete inventory of chromium carbides are low, the dissolution of partial carbides and diffusion of chromium, facilitated by rapid heating and cooling rates, will reduce sensitization at the grain boundaries. This tendency is evident in Fig. 11, where partial chromium carbides are observed at the grain boundaries, yet sensitization does not occur. Therefore, it can be inferred that even if chromium carbides precipitate due to exposure of the HAZ



(a)

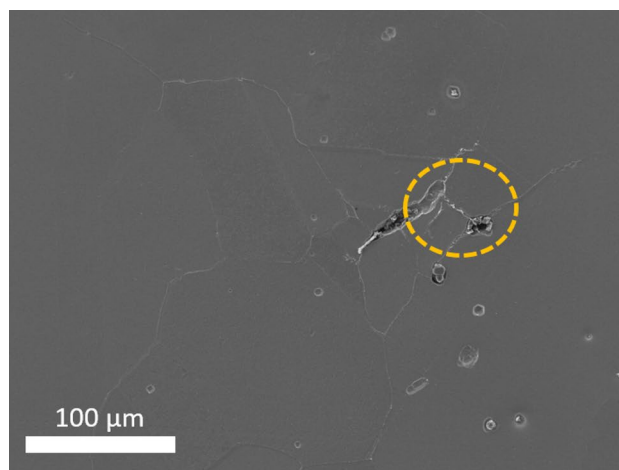


(b)

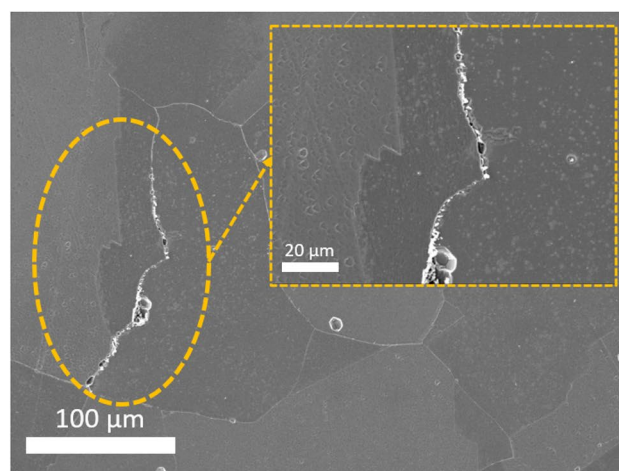
Fig. 10 DL-EPR curves of simulated specimens of a FH-L-2 and b FH-H-3 conditions with or without 1000 °C last cycle peak

to the sensitization temperature range, if the final thermal cycle reaches the austenitization temperature range (at least 1000 °C), then the short exposure time is sufficient for the precipitated carbides to dissolve, preventing sensitization from taking place.

Nevertheless, as previously discussed in the section about Fig. 3, where the heat history in the thickness direction led to material exposure to higher initial temperature regions compared to the surface, anticipating such an outcome becomes challenging. Even if exposure to the SA temperature range occurs during the initial phase, if subsequent thermal cycles subject the HAZ to the sensitization temperature range, sensitization is anticipated to occur irrespective of the location. When considering the choice of surface heat history conditions as an evaluation criterion, it is important to note



(a)



(b)

Fig. 11 SEM micrographs after DL-EPR tests of simulated specimens of a FH-L-2 and b FH-H-3 conditions with 1000 °C last cycle peak

that corrosion and IGSCC originate from the surface. Consequently, even if the HAZ area in the center of the base metal becomes sensitized, the impact on crack initiation might not be significant; however, it could accelerate the propagation of cracks. Therefore, effective management of thermal cycles within the center of the base metal is deemed essential.

### 4 Conclusions

The sensitization behavior of HAZ was investigated based on the exposure of different austenitic stainless steels with varying carbon content, namely A240 304L, A240 304H, and A182 F304H, to heat histories corresponding to different heat input levels and distances from the weld.



The Gleeble simulator replicated the heat histories, and tests were conducted under specified thermal cycles at the material's surface. The microstructure of both actual weld samples and specimens simulated through the Gleeble simulator confirmed the reproducibility of HAZ heat histories, as evidenced by the precipitation of  $M_{23}C_6$  carbides.

The DL-EPR test results indicated that higher carbon content led to elevated DOS values. Comparison of DOS values under L-2, H-2, and H-3 heat history conditions for 304H and F304H demonstrated that when the final thermal cycle peak reaches an austenitization temperature exceeding 1000 °C through rapid heating, partial carbide dissolution occurs and chromium diffuses at the grain boundaries, resulting in lowered DOS values.

This tendency is also evident through the reduction in DOS values, observed by reaching the solution annealing temperature due to rapid heating of the maximum temperature during the later stages of the heat history, even though L-1 and H-1 heat history conditions are exposed to the sensitization temperature range for a longer duration compared to other heat history conditions.

Furthermore, even in DL-EPR tests conducted on specimens subjected to L-2 and H-3 thermal cycles of sensitized F304H, a decrease in DOS values was observed with the addition of a last cycle peak at 1000 °C. This pattern was also confirmed by microstructure analysis.

Therefore, it was deemed that effectively managing the HAZ's thermal cycle to reach the final segment's SA temperature could contribute to improved corrosion and IGSCC resistance.

**Acknowledgements** This work was supported by the Institute for Korea Spent Nuclear Fuel (iKSNF) and Korea Institute of Energy Technology Evaluation and Planning (KETEP) grant funded by the Korean government's Ministry of Trade, Industry, and Energy (MOTIE) (No. 202104010 1002B) and Fundamental Research Program of the Korea Institute of Materials Science (KIMS) (Grant No. PNK 9870).

## Declarations

**Conflict of interest** On behalf of all authors, the corresponding author states that there is no conflict of interest.

**Open Access** This article is licensed under a Creative Commons Attribution 4.0 International License, which permits use, sharing, adaptation, distribution and reproduction in any medium or format, as long as you give appropriate credit to the original author(s) and the source, provide a link to the Creative Commons licence, and indicate if changes were made. The images or other third party material in this article are included in the article's Creative Commons licence, unless indicated otherwise in a credit line to the material. If material is not included in the article's Creative Commons licence and your intended use is not permitted by statutory regulation or exceeds the permitted use, you will need to obtain permission directly from the copyright holder. To view a copy of this licence, visit <http://creativecommons.org/licenses/by/4.0/>.

## References

1. C.S. Tedmon Jr., D.A. Vermilyea, J.H. Rosolowski, Intergranular corrosion of austenitic stainless steel. *J. Electrochem. Soc.* **118**, 192–202 (1971)
2. V. Kain, R.C. Prasad, P.K. De, Testing sensitization and predicting susceptibility to intergranular corrosion and intergranular stress corrosion cracking in austenitic stainless steels. *Corrosion* **58**, 15–37 (2002)
3. H. Sidhom, T. Amadou, H. Sahlaoui, C. Braham, Quantitative evaluation of aged AISI 316L stainless steel sensitization to intergranular corrosion: comparison between microstructural electrochemical and analytical methods. *Metall. Mater. Trans. A* **38A**, 1269–1280 (2007)
4. ASTM A262-10, *Standard Practice for Detecting Susceptibility to Intergranular Attack in Austenitic Stainless Steels* (ASTM International, West Conshohocken, 2010)
5. ASTM G108-94 (Reapproved 2010), *Standard Test Method for Electro-Chemical Reactivation (EPR) for Detecting Sensitization of AISI Type 304 and 304L Stainless Steels* (ASTM International, West Conshohocken, 2010)
6. G.H. Aydoğdu, M.K. Aydinol, Determination of susceptibility to intergranular corrosion and electrochemical reactivation behavior of AISI 316l type stainless steel. *Corros. Sci.* **48**, 3565–3583 (2006)
7. H. Sidhom, T. Amadou, C. Braham, Evaluation by the double loop electrochemical potentiokinetic reactivation test of aged ferritic stainless steel intergranular corrosion susceptibility. *Metall. Mater. Trans. A* **41**, 3136–3150 (2010)
8. T. Sourmail, C.H. Too, H.K.D.H. Bhadeshia, Sensitisation and evolution of Cr-depleted zones in Fe-Cr-Ni-C systems. *ISIJ Int.* **43**, 1814–1820 (2003)
9. H. Sahlaoui, K. Makhlof, H. Sidhom, J. Philibert, Effects of aging conditions on the precipitates evolution, chromium depletion and intergranular corrosion susceptibility of AISI 316L: experimental and modeling results. *Mater. Sci. Eng. A* **372**, 98–108 (2004)
10. E.C. Bain, R.H. Aborn, J.J.B. Rutherford, The nature and prevention of intergranular corrosion in austenitic stainless steels. *Trans. Am. Soc. Steel Treat.* **21**, 481–509 (1933)
11. T.M. Devine Jr., Influence of carbon content and ferrite morphology on the sensitization of duplex stainless steel. *Metall. Trans. A* **11**, 791–800 (1980)
12. R.V. Taivade, A.P. Patil, R.D. Ghugal, S.J. Patre, R.K. Dayal, Effect of welding passes on heat affected zone and tensile properties of AISI 304 stainless steel and chrome-manganese austenitic stainless steel. *ISIJ Int.* **53**, 102–109 (2013)
13. M.D. Toit, G.T. Van Rooyen, D. Smith, Heat-affected zone sensitization and stress corrosion cracking in 12% chromium type 1.4003 ferritic stainless steel. *Corros. Sci.* **63**, 395–404 (2007)
14. I. AghaAli, M. Farzam, M.A. Golozar, I. Danaee, The effect of repeated repair welding on mechanical and corrosion properties of stainless steel 316L. *Mater. Des.* **56**, 331–341 (2014)
15. C.M. Lin, H.L. Tsai, C.D. Cheng, C. Yang, Effect of repeated weld-repairs on microstructure, texture, impact properties and corrosion properties of AISI 304L stainless steel. *Eng. Fail. Anal.* **21**, 9–20 (2012)
16. R.-I. Hsieh, H.-Y. Liou, Y.-T. Pan, Effects of cooling time and alloying elements on the microstructure of the Gleeble-simulated heat-affected zone of 22% Cr duplex stainless steels. *J. Mater. Eng. Perform.* **10**, 526–536 (2001)
17. B. Silwal, L. Li, A. Deceuster, B. Griffiths, Effect of post weld heat treatment on the toughness of heat-affected zone for grade 91 steel. *Weld. J. Res. Suppl.* **92**, 80–87 (2013)



18. S. Kou, *Welding Metallurgy*, 3rd edn. (John Wiley & Sons, Hoboken, 2020)
19. S. Nakhodchi, A. Shokuhfar, S.A. Iraj, B.G. Thomas, Evolution of temperature distribution and microstructure in multipass welded AISI 321 stainless steel plates with different thicknesses. *J. Pressure Vessel Technol.* **137**, 061405 (2015)
20. R.C. Newman, Understanding the corrosion of stainless steel. *Corrosion* **57**, 1030–1041 (2001)
21. E.A. Trillo, L.E. Murr, A TEM investigation of  $M_{23}C_6$  carbide precipitation behaviour on varying grain boundary misorientations in 304 stainless steels. *J. Mater. Sci.* **33**, 1263–1271 (1998)
22. A.F. Candelaria, C.E. Pinedo, Influence of the heat treatment on the corrosion resistance of the martensitic stainless steel type AISI 420. *J. Mater. Sci. Lett.* **22**, 1151–1153 (2003)
23. S.A. Tukur, M.S. Dambatta, A. Ahmed, N.M. Muaz, Effect of heat treatment temperature on mechanical properties of the AISI 304 stainless steel. *Int. J. Innov. Res. Sci. Eng. Technol.* **3**, 9516–9520 (2014)
24. N. Parvathavarthini, R.K. Dayal, H.S. Khatak, V. Shankar, V. Shanmugam, Sensitization behaviour of modified 316N and 316L stainless steel weld metals after complex annealing and stress relieving cycles. *J. Nucl. Mater.* **355**, 68–82 (2006)
25. S. Papaethymiou, M. Bouzouni, R.H. Petrov, Study of carbide dissolution and austenite formation during ultra-fast heating in medium carbon chromium molybdenum steel. *Metals* **8**, 646–662 (2018)

**Publisher's Note** Springer Nature remains neutral with regard to jurisdictional claims in published maps and institutional affiliations.